Sensors and Materials, Vol. 35, No. 3 (2023) 1141–1148
MYU Tokyo

S & M 3235

Micro-electromechanical System Gas Sensors Based on CeO_2 Nanoparticles

Tang-Yu Lai,[1*] Guan-Cheng Chen,[2] and Yu-Jen Hsiao[2]

[1]R.O.C. Air Force Academy, No. Sisou 1, Jieshou W. Rd., Gangshan Dist., Kaohsiung City 820009, Taiwan
[2]Southern Taiwan University of Science and Technology,
No. 1, Nantai St., Yungkang Dist., Tainan City 710301, Taiwan

(Received October 23, 2022; accepted February 8, 2023)

Keywords: cerium oxide, MEMS gas sensor, hydrogen

In this study, X-ray diffraction (XRD) analysis was used to show that cerium oxide (CeO_2) nanoparticles have a face-centered cubic structure. CeO_2 thin films on micro-electromechanical system (MEMS) gas sensors, which are used to test their sensitivity to hydrogen (H_2), were prepared by dip coating. The test power of 116 mW (~300 °C) is the power consumption of different gas concentrations. Different gases such as NH_3, CO, and NO_2 were also tested and compared. The results showed that CeO_2 has a higher response at 50 ppm than at other concentrations. The structure of the CeO_2 material and its reaction mechanism with H_2 were examined and discussed.

1. Introduction

With industrial development, air pollution, which severely affects the environment and personal health, is becoming increasingly serious. Air quality is an important issue that cannot be ignored today. Air pollutants can be divided into outdoor and indoor emissions or formations. The most common outdoor and indoor air pollutants originate from the use of fossil fuels for industrial and residential purposes, including gaseous SO_2, NO_2, CO, and volatile organic compounds, as well as particulate matter, which has attracted considerable attention recently. These air pollutants are major contributors to the global disease burden.[1–4]

There is a growing interest in developing clean and sustainable energy carriers as an alternative to fossil fuels. Hydrogen gas, as a renewable and clean energy source, can prevent air pollution due to conventional fuels. However, hydrogen (H_2) is a colorless and odorless gas and is flammable. It is difficult for people to detect the presence of high concentrations of H_2 in the environment, resulting in exposure to high-risk environments.[5–7] Therefore, developing sensitive and accurate gas sensors for H_2 production and storage is critical. Metal oxide semiconductors (MOSs) have been studied extensively and are the materials used for gas sensing. When a gas reacts with the MOS material, the sensor can detect the gas based on the change in resistance.[8–12] Unlike other sensing methods, this method of observing resistance

*Corresponding author: e-mail: LTY0131@gmail.com
https://doi.org/10.18494/SAM4239

ISSN 0914-4935
https://myukk.org/

changes has the advantages of high sensitivity, wide operating temperature range, low cost, easy fabrication, fast response, and low power consumption. Several MOS materials can sense the reaction of H_2 production in gas detection. Researchers have demonstrated cerium oxide (CeO_2), a rare-earth resource, as a promising gas-sensing material because of its large redox properties and high oxygen storage capacity.[13–15]

In this study, a micro-electromechanical system (MEMS) heating platform structure and double gun sputtering were used to prepare a CeO_2 film gas sensor. After the CeO_2 membrane was produced, the film composition was determined and gas detection was performed, followed by the response analysis of the H_2 gas. After monitoring the sensitivity levels to H_2, the sensing sensitivity levels to other gases (NH_3, CO, and NO_2) were compared to evaluate the performance of the CeO_2 film gas sensor.

2. Materials and Methods

CeO_2 was prepared by a step-by-step method consisting of a nanogrinding and dispersion machine process.[16,17] A schematic of the MEMS is shown in Fig. 1(a), which shows the semiconductor cavity structure, microheater, and sensing material.

The sensor uses a p-type 400-μm-thick silicon wafer as the substrate. A 400-nm-thick Ti layer and a 50-nm-thick Au layer were deposited on top of the established pattern. In turn, the physical vapor deposition of Ti and Pt layers was carried out. A positive photoresist (PR) was used for spin coating onto the release layer. Finally, SF6 plasma surface etching was performed

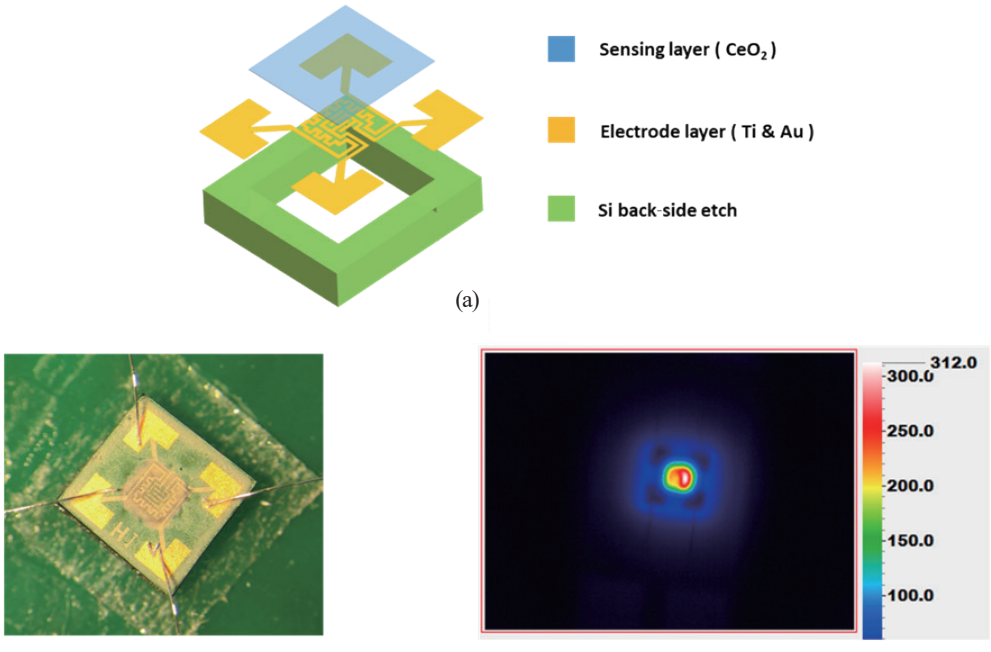

(a) (b) (c)

Fig. 1. (Color online) (a) Schematic of an exploded view of the gas sensor structure. (b) Top view of the sensor under a microscope. (c) Temperature distribution of sensing area under Thermal Image Camera (TIC).

to form structures on the reverse side. Microheaters work on the basis of the thermal principles of the wire. The sensing layer of CeO_2 was deposited by dip coating [Fig. 1(b)]. When the powers of the microheater shown in Fig. 1(c) are 28, 49, 70, 92, and 116 mW in sequence, the corresponding temperatures of the sensing film are 100, 150, 200, 250, and 300 °C, respectively. As the temperature continues to increase, the response also increases.

Gas measurements were performed in a vacuum chamber where the measured gas was inserted to record sensing parameters from the MEMS device. The MEMS microheater has four electrodes, two for sensing and two for heating. The sensing electrodes were connected to "Keithley-2400" resistance measuring equipment and the heating electrodes were connected to "MOTECH LPS-305" for the power supply. The change in resistance as the gas entered the chamber was recorded in "lab view" software, and the obtained data were presented as graphical representations.

3. Results and Discussion

The crystalline structures and compositions of the samples were characterized using X-ray diffraction (XRD) (Fig. 2). The results show the XRD patterns of CeO_2, which is an obvious crystal phase of cerium cubic fluorite oxide (JCPDF file no. 34–0394), and the crystal planes of fluorite phases are (111), (200), (220), (311), (222), and (400), corresponding to the peaks. The Scherrer formula [Eq. (1)] was used to calculate the full widths at half maximum for the average crystallite size. We referred to a report[18] for calculation using the main peak (111) reflection (2θ = 26°), in which the morphological parameter or shape factor for spherical particles (k) is 0.94 nm^{-1}, the wavelength (λ) of the radiograph is 0.154 nm, and the crystallite size of the nanostructures is 8.49 nm.

$$D = k\lambda / \cos\theta \tag{1}$$

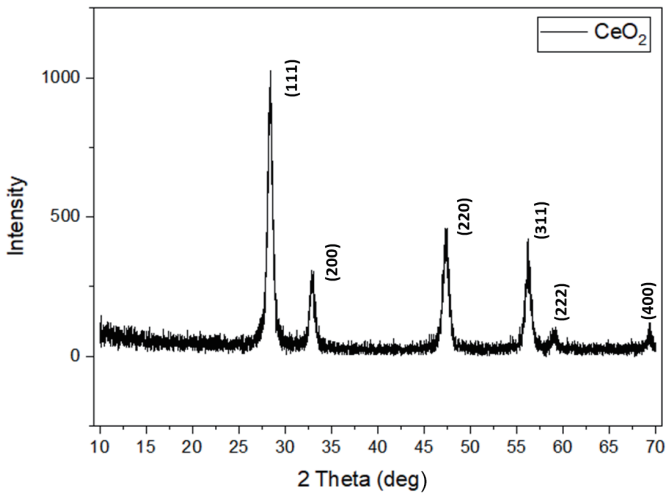

Fig. 2. XRD patterns of CeO_2.

The distribution of crystallites of similar size was observed using the TEM image. The TEM image of CeO_2 with an inset of a select area electron diffraction (SAED) pattern is shown in Fig. 3. TEM images show that the nanocrystals have high crystallinity, there are no obvious impurities, and the CeO_2 nanoparticles are of different sizes. This is because some small particles combine to form large particles after being baked on the hot plate, and fine pores are generated between the particles, which benefits the gas-sensing surface area and improves the sensing sensitivity. The above results agree with previous studies.[19–21]

Gas sensing was measured in a closed cavity. After the testing gas (H_2 or other gases) was injected into the cavity, the sensing material of the CeO_2 membrane responded and decreased the resistance. When testing gas-out and air-in, the resistance increased to its original value. We recorded the change in resistance as the concentration increased from 10 to 50 ppm and the temperature ranged from 100 to 300 ℃. The response was calculated as

$$Response(\%) = \frac{R_{gas} - R_{air}}{R_{gas}} \times 100\%. \quad (2)$$

Figure 4 shows the response curves of a CeO_2 membrane with different H_2 concentrations at different temperatures. The results show that the CeO_2 membrane has good response to H_2, and the change in resistance can be measured quickly when gas-in and gas-out take place. As the H_2 concentration increased from 10 to 50 ppm, the response increased from 10 to 70% [Fig. 4(a)]. As the gas concentration increased, the sensing sensitivity increased significantly. Furthermore, as the temperature increased, the response speed and stability improved, with the optimal temperature being 300 ℃ [Fig. 4(b)–(h)]. Additionally, the sensing results were perfectly reproduced after repeated measurements, indicating that the CeO_2 membrane gas sensing is highly stable. We conducted sensing tests for various gases to explore the gas sensing of CeO_2. The responses of the CeO_2 membrane with various gases (3 ppm) at 300 ℃ are shown in Fig. 5. The results show that the CeO_2 membrane has a low responses for NH_3, CO, and NO_2, and the obtained values are all less than 10%. That is, the CeO_2 membrane has high selectivity to H_2.

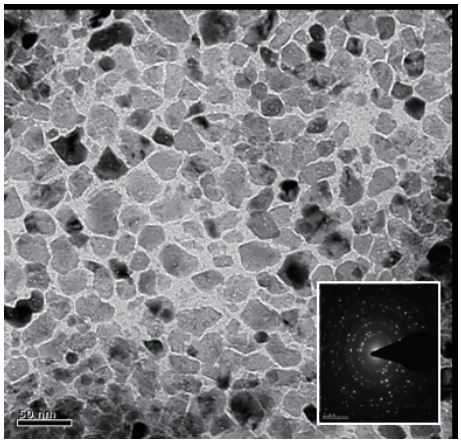

Fig. 3. TEM image of CeO_2. The inset is the SAED pattern.

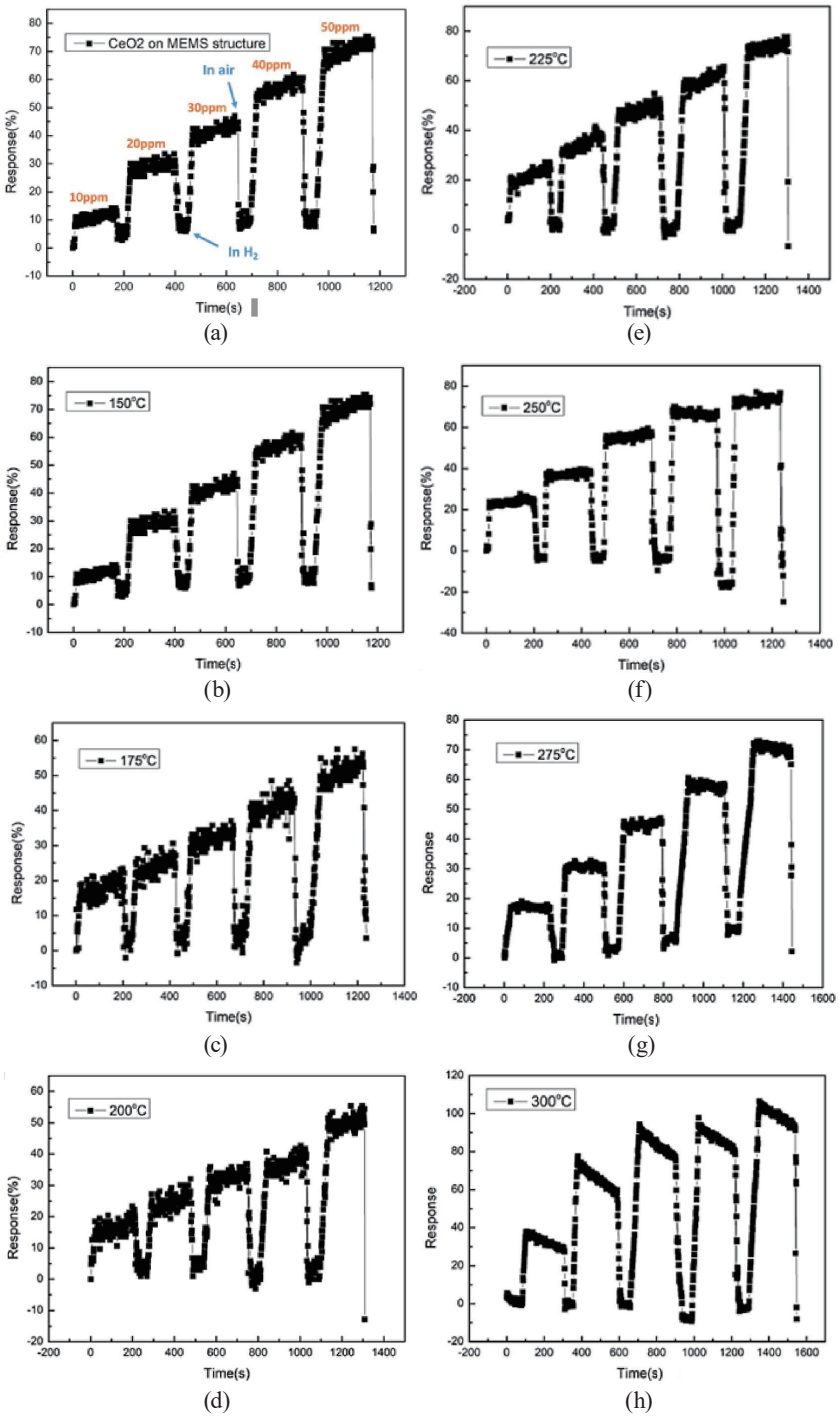

Fig. 4. (Color online) Response curves of CeO2 membrane with different H_2 concentrations at different temperatures from 100 to 300 °C.

Figure 6 shows the sensing mechanism of a CeO_2 membrane at H_2 ambient. CeO_2 is an n-type MOS. When the CeO_2 membrane is exposed to the atmosphere, it adsorbs oxygen molecules and forms oxygen ions (O^-) on the surface of the material. If H_2 is added to the

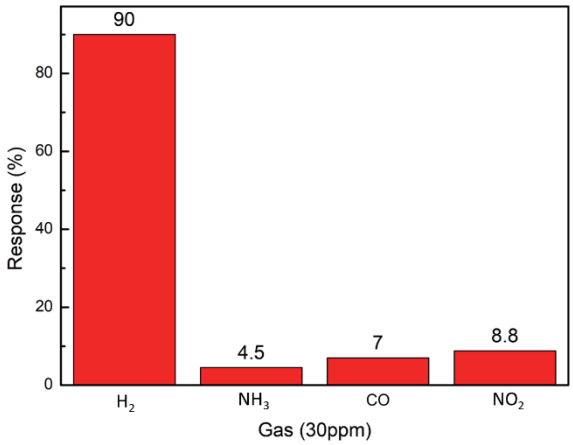

Fig. 5. (Color online) Responses of CeO_2 membrane with various gases (50 ppm) at 300 °C.

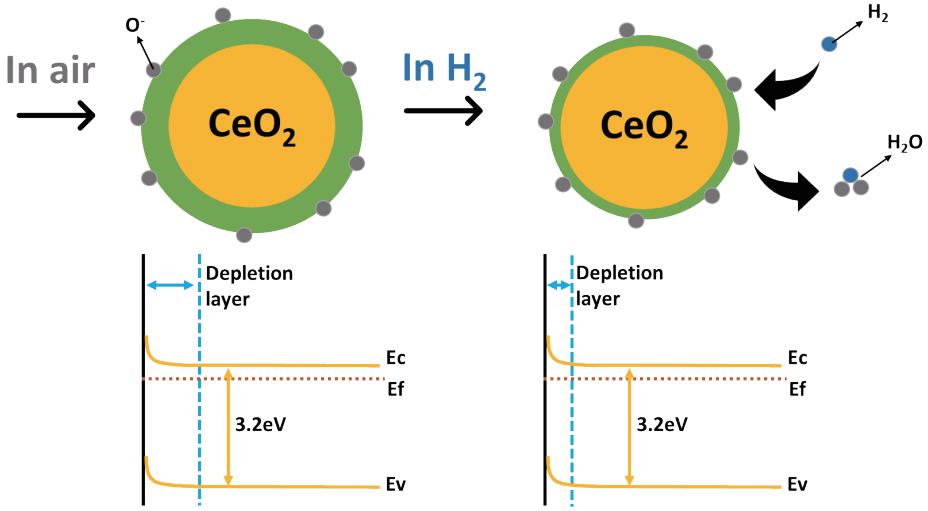

Fig. 6. (Color online) Sensing mechanism of CeO_2 membrane at H_2 ambient.

ambient atmosphere, surface O^- will react with H_2 to form water (H_2O) and electrons (e^-), and the reaction is

$$H_2 + O^- \rightarrow H_2O + e^-. \quad (3)$$

At this point, the electron concentration in the conduction band of ceria decreases, and an electron depletion layer (EDL) is formed on the surface, increasing the resistance (R_{air}). In this study, the exposure of CeO_2 to H_2 gas causes a reduction reaction, where the trapped electrons are released back into the conduction band and the width of the EDL decreases, resulting in a decrease in sensor resistance (R_{gas}).[22,23]

4. Conclusions

In this study, the power consumption and gas concentration variables related to the sensitivity and material properties of the CeO_2 film were discussed. At 116 mW (~300 °C), the sensitivity increased with the H_2 concentration. Moreover, its sensitivity was compared with other gases. When tested at the same temperature and concentration, the maximum response of H_2 was 90% and those of the other three gases were less than 10%. The MEMS gas sensors of the CeO_2 membrane have high selectivity to H_2.

Acknowledgments

The authors acknowledge the support by the National Science and Technology Council, Taiwan under grant number 111-2221-E-013-003.

References

1 M. C. Turner, Z. J. Andersen, A. Baccarelli, W. Diver, R. Diver, S. M. Gapstur, C. A. Pope, D. Prada, J. Same, G. Thurston, and A. Cohen: CA: A Cancer J. Clinicians **70** (2020) 460. https://doi.org/10.3322/caac.21632
2 J. Lelieveld, J. S. Evans, M. Fnais, D. Giannadaki, and A. Pozzer: Nature **525** (2015) 367. https://doi.org/10.1038/nature15371
3 M. D. Gwynne: Environ. Conserv. **9** (1982) 35. https://doi.org/10.1017/S0376892900019469
4 D. Loomis, W. Huang, and G. Chen: Chinese J. Cancer **33** (2014) 189. https://doi.org/10.5732/cjc.014.10028
5 N. Sazali: Int. J. Hydrogen Energy **45** (2020) 18753. https://doi.org/10.1016/j.ijhydene.2020.05.021
6 H. Ishaq, I. Dincer, and C. Crawford: Int. J. Hydrogen Energy **47** (2022) 26238. https://doi.org/10.1016/j.ijhydene.2021.11.149
7 R. Moradi and K. M. Groth: Int. J. Hydrogen Energy **44** (2019) 12254. https://doi.org/10.1016/j.ijhydene.2019.03.041
8 X. Gao and T. Zhang: Sens. Actuators, B **277** (2018) 604. https://doi.org/10.1016/j.snb.2018.08.129
9 B. Yang, N. V. Myung, and T. Tran: Adv. Electron. Mater. **7** (2021) 2100271. https://doi.org/10.1002/aelm.202100271
10 T. Lai, T. Fang, Y. Hsiao, and C. Chan: Vacuum **166** (2019) 155. https://doi.org/10.1016/j.vacuum.2019.04.061
11 T. Lai, T. Fang, Y. Hsiao, and E. Kuo: Curr. Nanosci. **16** (2020) 187. https://doi.org/10.2174/1573413715666190710165825
12 Y. Hsiao, Z. Shi, Y. Nagarjuna, Z. Huang, T. Lai, and S. Wu: ECS J. Solid State Sci. Technol. **11** (2022) 057002. https://iopscience.iop.org/article/10.1149/2162-8777/ac71c7/
13 P. S. Chauhan and S. Bhattacharya: Int. J. Hydrogen Energy **44** (2019) 26076. https://doi.org/10.1016/j.ijhydene.2019.08.052
14 P. Li, B. Wang, C. Qin, C. Han, L. Sun, and Y. Wang: Ceramics Int. **46** (2020) 19232. https://doi.org/10.1016/j.ceramint.2020.04.261
15 H. Bi, L. Zhang, Y. Xing, P. Zhang, J. Chen, J. Yin, and L. Bie: Sens. Actuators, B **330** (2021) 129374. https://doi.org/10.1016/j.snb.2020.129374
16 Y. Nagarjuna and Y. Hsiao: J. Electrochem. Soc. **169** (2022) 077502. https://iopscience.iop.org/article/10.1149/1945-7111/ac7c40/meta
17 Y. Nagarjuna and Y. Hsiao: Coatings **10** (2020) 945. https://doi.org/10.3390/coatings10100945
18 C. Yamerson, M. F. Angie, P. Jemina, B. Yéssica, J. A. Guerra, and R. A. Juan: Nanomaterials **11** (2021) 2311. https://doi.org/10.3390/nano11092311
19 C. Papadopoulos, K. Kappis, J. Papavasiliou, J. Vakros, M. Kuśmierz, W. Gac, Y. Georgiou, Y. Deligiannakis, and G. Avgouropoulos: Catal. Today **355** (2020) 647. https://doi.org/10.1016/j.cattod.2019.06.078
20 S. Song, C. Zhang, Y. Lou, Y. Wu, L. Wang, Y. Guo, W. Zhan, and Y. Guo: J. Rare Earths **38** (2020) 891. https://doi.org/10.1016/j.jre.2020.04.021

21 C. Italiano, J. Llorca, L. Pino, M. Ferraro, V. Antonucci, and A. Vita: Appl. Catal. B **264** (2020) 118494. https://doi.org/10.1016/j.apcatb.2019.118494
22 S. Hussain, N. Aslam, X. Yang, M. S. Javed, Z. Xu, M. Wang, G. Liu, and G. Qiao: Ceram. Int. **44** (2018) 19624. https://doi.org/10.1016/j.ceramint.2018.07.212
23 S. Prabakaran and J. B. B. Rayappan. Sci. Lett. J. **4** (2015) 126. http://www.cognizure.com/abs/200638572.aspx